Journal of Solid State Chemistry 183 (2010) 1221–1225

Contents lists available at ScienceDirect

Journal of Solid State Chemistry

journal homepage: www.elsevier.com/locate/jssc

$K_2Fe_2B_2O_7$: A transparent nonlinear optical crystal with frustrated magnetism

Yonggang Wang [a,b], R.K. Li [a,*]

[a] Beijing Center for Crystal Research and Development, Key Laboratory of Functional Crystals and Laser Technology, Technical Institute of Physics and Chemistry, Chinese Academy of Sciences, Beijing 100190, China
[b] Graduate University of Chinese Academy of Sciences, Beijing 100049, China

ARTICLE INFO

Article history:
Received 13 January 2010
Received in revised form
19 March 2010
Accepted 28 March 2010
Available online 2 April 2010

Keywords:
Ferroborate
NLO
Triangular lattice
Frustration
Spin-glass

ABSTRACT

A new noncentrosymmetric ferroborate crystal, $K_2Fe_2B_2O_7$, has been grown from high temperature melt. Structure solution from single crystal X-ray diffraction shows that the title compound crystallizes in a trigonal space group $P321$ with cell dimensions of $a=8.7475(12)$ Å and $c=8.5124(17)$ Å. In the structure, FeO_4 tetrahedron shares its three basal oxygen atoms with BO_3 triangles forming a two-dimensional layer in the ab plane and the layers are connected by the apical Fe–O bonds along the c direction. The crystal is transparent in the visible and near infrared region from 500 to 2000 nm with three pronounced absorption bands ascribed to d–d transitions of tetrahedrally coordinated Fe^{3+} ions. Though, structurally analog to $K_2Al_2B_2O_7$, the further twisting of the BO_3 groups between adjacent layers reduces its optical nonlinearity to a second-harmonic generation intensity of about 0.4 times that of KDP. Spin-glass behavior is observed at 20 K which is probably due to geometrically magnetic frustration of the triangular Fe net in the ab plane.

1. Introduction

The large family of borate compounds, acting as a "*chemical playground*" of structure design for functional materials, has provided an expansive area of research for over 50 years owing to the extremely wide variability of borate crystal chemistry and their good chemical stability [1–3]. Since the advent of low-temperature BaB_2O_4 (BBO) and LiB_3O_5 (LBO) as two efficient nonlinear optical (NLO) materials [4,5], various main-group metal borates have been discovered and suggested for NLO applications, especially in UV region because of their high UV transmittance and high damage threshold. Besides, transition-metal borates and rare-earth-metal borates integrating in one crystalline matrix with two or more physical features are also the focus of both theoretical and experimental studies. The presence of d- or f-block elements in these borates results in a variety of technologically important properties, and they emerge as important multifunctional materials when given optical characteristics are combined with magnetic or electric properties. Metal borates of the general formula $RM_3(BO_3)_4$ (R=Y, La–Lu; M=Al, Ga, Fe, Cr, Sc) [6–10], crystallizing in the trigonal structure of the mineral huntite $CaMg_3(CO_3)_4$ type (space group $R32$), are the most widely developed system. They are classed as new-generation materials for lasers in respect that they exhibit both luminescence and second-harmonic generation (SHG) properties. Nd-doped $YAl_3(BO_3)_4$ and $GdAl_3(BO_3)_4$ crystals as the two representatives of this family have been widely studied and applied in self-frequency-doubling laser sources [11–14]. Another interesting aspect of $RM_3(BO_3)_4$ system is that when M is a transition metal element (like Fe or Cr), the well separated MO_6 helical magnetic chains interact mutually and also interact with the magnetic rare earth ions leading to complicated magnetic behaviors which endue them with promising magneto-optical and other multi-ferroic properties [15–17].

There are only a few borates containing trivalent iron ion (so-called ferroborate) showing magnetic ordering: $FeBO_3$ [18], Fe_3BO_6 [19], $RFe_3(BO_3)_4$ (R=Y, La–Lu) [20], and $Fe(M^{II}O)_n(BO_3)$ (M=Co, Mn, Zn, n=1; M=Cu, Ni, n=2) [21]. As a well-known weak ferromagnet, iron borate $FeBO_3$ represents a rare example of a magnetically ordered ferric oxide with high transparency in the visible spectral region and important magneto-optical properties [18d,18e]. When we concentrated on the study of d–d transitions in Fe-doped $K_2Al_2B_2O_7$ (KABO) crystals [22], we found that as the content of iron increases, X-ray diffraction peaks shift towards lower 2θ values from pure KABO gradually, which indicates the formation of $K_2(Fe_xAl_{1-x})_2B_2O_7$ solid solution, whereas the crystal system maintains. At the end, a new compound $K_2Fe_2B_2O_7$, structurally analog to KABO with the aluminum fully substituted by iron, was obtained. $K_2Fe_2B_2O_7$ crystal shows high transparency in the visible and IR region, considerable SHG efficiency and interesting magnetic properties.

2. Experiment section

2.1. Crystal growth and X-ray diffraction

Single crystals of $K_2Fe_2B_2O_7$ were grown by spontaneous nucleation in a platinum crucible from the melt of analytical

* Corresponding author. Fax: +86 10 82543709.
E-mail address: rkli@mail.ipc.ac.cn (R.K. Li).

0022-4596/$ - see front matter © 2010 Elsevier Inc. All rights reserved.
doi:10.1016/j.jssc.2010.03.037

reagent (AR) grade K_2CO_3, Fe_2O_3 and H_3BO_3 in molar ratios of K:Fe:B=1:1:1.2. The melt was cooled from 900 to 800 °C at a rate of 2 °C/h and then to room temperature with power off. Platelet crystals appeared at the surface in the crucible and they were mechanically separated from the solution surface. Typical products consist transparent, yellowish crystal sheets with size up to $2.5\times2.5\times0.2\,mm^3$ (see Appendices, Fig. A1).

The structure of $K_2Fe_2B_2O_7$ was determined by single-crystal X-ray diffraction on a Rigaku AFC10 diffractometer equipped with Mo$K\alpha$ radiation ($\lambda=0.71073$ Å). Data were collected at low temperature (93 K) with θ range from 3.60° to 27.47°. A total of 4534 reflections were measured, of which 874 unique ones were used for the structure solution. The crystal structure was solved and refined by SHELXS-97 and SHELXL-97 packages [23], adopting the structural parameters of KABO as an initial structure model. Final agreement indices of $wR2=0.0540$ and $R1=0.0282$ were obtained. The final difference electron-density map shows a highest peak of $0.50\,eÅ^{-3}$ located 0.78 Å from O1 and a deepest hole of $-0.67\,eÅ^{-3}$ located 0.32 Å from Fe1. Further crystallographic parameters and the refined structural data are provided in Table 1.

2.2. Physical property measurements

Optical transmittance spectrum was recorded with a Lambda 900 UV–VIS–NIR (Perkin-Elmer) spectrophotometer in the region of 185–2000 nm and the thermal stability of the title compound was analyzed with differential thermal analysis (DTA) under static air in a WCR-2A DTA instrument. For the powder SHG intensity measurement, a Nd^{3+}:YAG laser of wavelength 1064 nm was used as incident light and the frequency-doubled outputs were recorded using KDP as a reference. Since the powder SHG efficiency depends strongly on particle size based on the Kurtz–Perry method [24], the $K_2Fe_2B_2O_7$ crystals were ground and sieved into distinct particle sizes varying from 20 to 150 μm.

Temperature dependence of the *dc* magnetic susceptibility was measured on a superconducting quantum interference device magnetometer (SQUID, Quantum Design) under field cooled (FC) and zero field cooled (ZFC) conditions. Data were collected over the temperature range 5–400 K with an applied field of 1000 G.

3. Results and discussion

3.1. Structure

$K_2Fe_2B_2O_7$ crystallizes in the trigonal space group *P*321 with lattice parameters $a=b=8.7475(12)$ Å and $c=8.5124(17)$ Å and exhibits a layered structure composed by the arrangement of BO_3 triangles and tetrahedral FeO_4 groups (shown in Fig. 1). There are three crystallographically independent Fe sites leading to three different types of distorted FeO_4 units and forming two types of apical sharing tetrahedral FeO_4 pairs with 180° Fe1–O1–Fe1 and Fe_2–O_2–Fe_3 bonds. It is found that the three tetrahedral FeO_4 units are almost identical with little variations of the basal Fe–O bonds ranging from 1.868(2) to 1.877(2) Å and the apical Fe–O bonds varying from 1.7917(8) to 1.800(3) Å. The observation of significant shortening of the apical bonds can also be found in KABO [25], where the distances of the basal and apical Al–O bonds are observed as 1.756 and 1.700 Å, respectively. The bottom surfaces of all the FeO_4 tetrahedra share corners with three adjacent BO_3 triangles to form six-membered rings, which produce a triangular Fe lattice parallel to the *ab* crystal plane. These two groups formed a nearly planar $[Fe_3B_3O_6]$ framework with all the planes of BO_3 groups approximately perpendicular to the *c* axis. The average bond length for B–O is 1.374 Å and the mean O–B–O bond angle is close to 120°, which are in accordance with the ideal BO_3 triangle having a B–O distance and O–B–O angle of 1.368 Å and 120° [26]. The selected inter-atomic distances and bond angles of $K_2Fe_2B_2O_7$ are shown in Table 2.

$K_2Fe_2B_2O_7$ is structurally closely related to KABO, both of which contain planar $[BO_3]^{3-}$ groups as their major NLO active units [25b,25c]. The contrasting BO_3 groups' arrangements in the unit cells of $K_2Fe_2B_2O_7$ and KABO are shown in Fig. 2. It is found that in $K_2Fe_2B_2O_7$ structure, BO_3 groups are twisted about 50° from those of adjacent layers, whereas the angle of twist is only 40° in KABO. The further twisting of BO_3 triangles in $K_2Fe_2B_2O_7$ may be attributed to the longer in-plane Fe–O bonds than that of the Al–O bonds. In order to host the much longer Fe–O bonds in a K–O set lattice, the BO_3 triangles are forced to twist, giving a much bent Fe–O–B bonds. According to the anionic group model for borate compounds proposed by Chen et al. [27], the BO_3 groups are considered to be the most basic structural units responsible for optical nonlinearity, and the bulk NLO properties can be calculated by summating their respective contributions. Consequently, the SHG coefficient of $K_2Fe_2B_2O_7$ can be calculated as $d_{11}=-0.315$ pm/V, which is smaller than that of KABO (calculated: $d_{11}=0.585$ pm/V, experimental: $d_{11}=0.46$ pm/V) [28,29]. Fig. 3 shows the experimental SHG signal intensities of $K_2Fe_2B_2O_7$ powder with different particle sizes relative to KDP standard and it gives a maximum value of about 0.4 times that of KDP despite that $K_2Fe_2B_2O_7$ possesses some extent of absorption at 532 nm. This is approximately half that of KABO powder (0.9 times of KDP) with the same particle size, which is in good agreement with the calculation results given above. The experiment and calculation show that the significant reduction of SHG coefficient of $K_2Fe_2B_2O_7$ with respect to KABO can be solely attributed to the larger twisting of the BO_3 groups, while the absorption caused by Fe^{3+} ions contributes to a much lesser extent. It is worth mentioning that when the twisting angle goes towards 60°, all the contributions of the BO_3 groups to the SHG coefficients will be cancelled. Compared with KABO crystal, $K_2Fe_2B_2O_7$ has a lower congruent melting point at about 851 °C (see Appendices, Fig. A2) which makes it possible to be grown by the Czochralski method. In addition, another alkali metal borate $Rb_2Fe_2B_2O_7$ has also been synthesized, which possesses similar XRD peaks (see Appendices, Fig. A3) but exhibits no SHG effects.

One of the other interesting aspects of the structure as mentioned above is that all the three Fe^{3+} ions sit in tetrahedrally coordinated environments. The lack of inversion symmetry relaxes the parity selection rule, thus leading to the emergence of some spin-forbidden bands dominating the transmittance spectrum of $K_2Fe_2B_2O_7$ in the visible region (shown in Fig. 4). These bands can be ascribed to *d*–*d* transitions of tetrahedrally

Table 1
Refined structural data of $K_2Fe_2B_2O_7$ at 93 K.

Atom	*x*	*y*	*z*	U_{eq} (Å^2)
Fe1	0	0	0.71048(8)	0.0045(2)
Fe2	2/3	1/3	0.80960(8)	0.0049(2)
Fe3	1/3	2/3	0.76756(8)	0.0051(2)
K1	0.68190(11)	0	0	0.0097(2)
K2	0.64708(11)	0	0.5	0.0097(2)
O1	0	0	0.5	0.0132(11)
O2	1/3	2/3	0.9789(4)	0.0165(9)
O3	0.5630(3)	0.7391(3)	0.6991(3)	0.0103(5)
O4	0.8978(3)	0.4124(3)	0.7429(3)	0.0109(5)
O5	0.2283(3)	0.0669(3)	0.7810(3)	0.0101(5)
B	0.0010(4)	0.3358(5)	0.7411(4)	0.0069(8)

Space group: *P*321 $a=b=8.7475(12)$ Å and $c=8.5124(17)$ Å.
$R1=0.0282$ and $wR2=0.0540$ for all data.

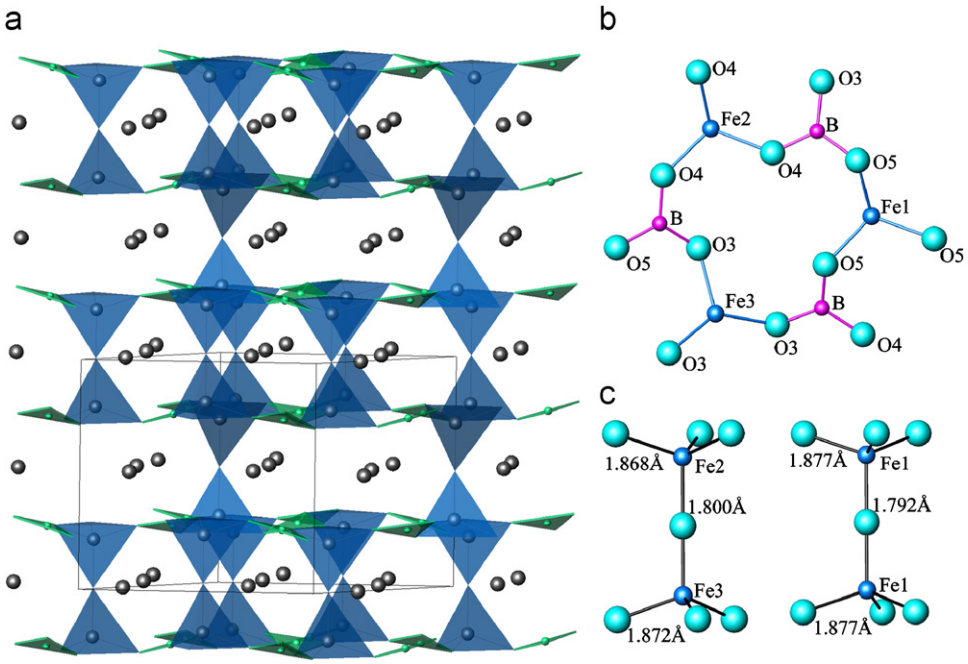

Fig. 1. (a) Crystal structure of $K_2Fe_2B_2O_7$ showing FeO_4 tetrahedral groups in blue and BO_3 trigonal groups in green (Fe, blue spheres; B, green spheres; K, black spheres; Oxygen atoms omitted for clarity). (b) Ball-and-stick representation of individual six-membered ring containing three BO_3 and three FeO_4 units and (c) the two different types of FeO_4 tetrahedral pairs. (For interpretation of the references to colour in this figure legend, the reader is referred to the web version of this article.)

Table 2
Selected inter-atomic distances (Å) and bond angles (°) for $K_2Fe_2B_2O_7$.

K1–O2(× 2)	2.9901(7)	K2–O1^{i}	3.0872(10)
K1–O3(× 2)	3.237(2)	K2–O3(× 2)	2.635(2)
K1–O4(× 2)	3.006(2)	K2–O4(× 2)	2.730(2)
K1–O5(× 2)	2.682(2)	K2–O5(× 2)	3.232(2)
In FeO_4 Tetrahedra			
Fe1–O1	1.7917(8)	O1–Fe1–O5	108.66(7)
Fe1–O5(× 3)	1.877(2)	O5–Fe1–O5	110.27(7)
Fe2–O2^{ii}	1.800(3)	O4–Fe2–O2^{ii}	107.69(7)
Fe2–O4(× 3)	1.868(2)	O4–Fe2–O4	111.19(7)
Fe3–O2	1.799(3)	O3–Fe3–O2	108.15(7)
Fe3–O3(× 3)	1.872(2)	O3–Fe3–O3	110.76(7)
In BO_3 Triangles			
B–O3^{iii}	1.379(4)	O3^{iii}–B–O4	118.8(3)
B–O4^{iv}	1.367(4)	O4^{iv}–B–O5^{v}	121.1(3)
B–O5^{v}	1.375(4)	O3^{iii}–B–O5^{v}	120.1(3)

Symmetry codes: (i) $x+1, y, z$, (ii) $y, x, -z+2$, (iii) $-x+y, -x+1, z$, (iv) $x-1, y, z$ and (v) $-y, x-y, z$.

coordinated Fe^{3+} ions, $^6A_1 \rightarrow {}^4T_2$ (^4D) at 442 nm, $^6A_1 \rightarrow {}^4T_2$ (^4G) at 510 nm and $^6A_1 \rightarrow {}^4T_1$ (^4G) at 625 nm, respectively. These assignments are also in agreement with the *d–d* transitions of partially Fe^{3+} doped KABO crystal [22]. Although the existence of Fe always results in absorptions in the UV and visible region, such Fe-containing materials (e.g. $FeBO_3$, $RFe_3(BO_3)_4$, $Fe(IO_3)_3$ [30]) are still widely studied for magnetic and NLO applications at longer wavelength in visible and infrared region. It is noteworthy that $K_2Fe_2B_2O_7$ is optically transparent from 500 to 2000 nm (Fig. 4) and this gives it practicability for potential optical applications in the future.

3.2. Magnetism

The temperature dependence of the magnetic susceptibilities of $K_2Fe_2B_2O_7$ in both ZFC and FC conditions is shown in Fig. 5. Above 30 K, $K_2Fe_2B_2O_7$ exhibits paramagnetic behavior. Unfortunately, in respect that the powder sample of the title compound is easy to decompose in atmosphere and only a small quantity (7 mg) of single crystals available for measurement relative to the assistant diamagnetic materials, the exact value of effective magnetic-moment (μ_{eff}) for each Fe^{3+} ion cannot be obtained here. A susceptibility maximum in ZFC curve is observed at 20 K, which can be attributed as the evidence of spin-glass at the freezing temperature (T_f=20 K), as the ZFC and FC susceptibility curves diverge at T_f. Magnetic ions embedded in borates can often form a triangular lattice with layered structures owing to the planar BO_3 triangular groups. Materials featuring such triangular lattices consisting of corner-sharing or edge-sharing triangles are predicted to have no long range order in the lowest temperature due to competing AFM coupling between the nearest-neighbor spins [31–33]. In the past few years, several transition-metal borates have been found to show magnetic frustrations, such as $LiMnBO_3$ with a triangular magnetic lattice, $YCa_3(MnO)_3(BO_3)_4$, and $Ca_4(MnO)_3(BO_3)_3CO_3$ with a Kagomé lattice [34–36], particularly. The interaction between the linear Fe–O–Fe bonds connecting the triangular layer can be expected to be AFM through 180° superexchange and the Fe–O–B–O–Fe pathway in the triangular layer (with nearest Fe–Fe distance of 5.064 Å) is also possibly AFM. It is probably the latter in-plane AFM interaction, which gives rise to the spin frustration. Further magnetic structural studies (e.g. neutron diffraction) are necessary to reveal the actual magnetic interactions among the magnetic ions within the plane and among the layers.

4. Conclusion

A new noncentrosymmetric ferroborate, $K_2Fe_2B_2O_7$, has been prepared as single crystal form and is found to crystallize in the trigonal space group *P*321. It possesses a layered structure composed of FeO_4 tetrahedra and BO_3 triangle groups forming a triangular Fe lattice in the *ab* plane. $K_2Fe_2B_2O_7$ crystal is

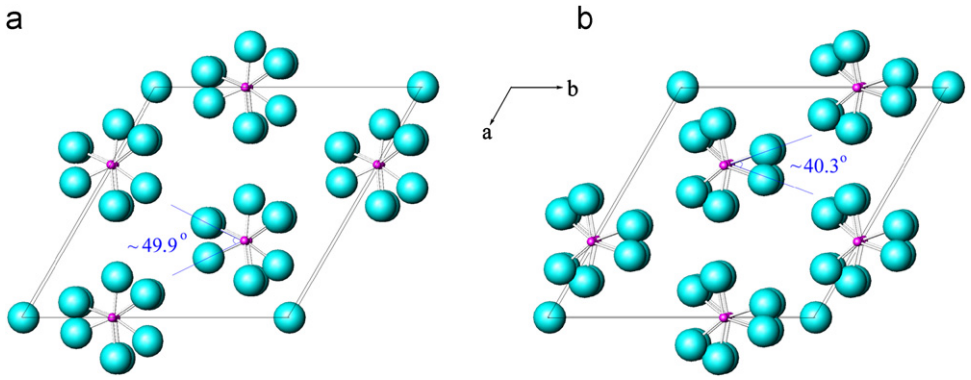

Fig. 2. Arrangement of BO_3 triangles in $K_2Fe_2B_2O_7$ (a) and KABO (b) crystals viewed along the *c* axis.

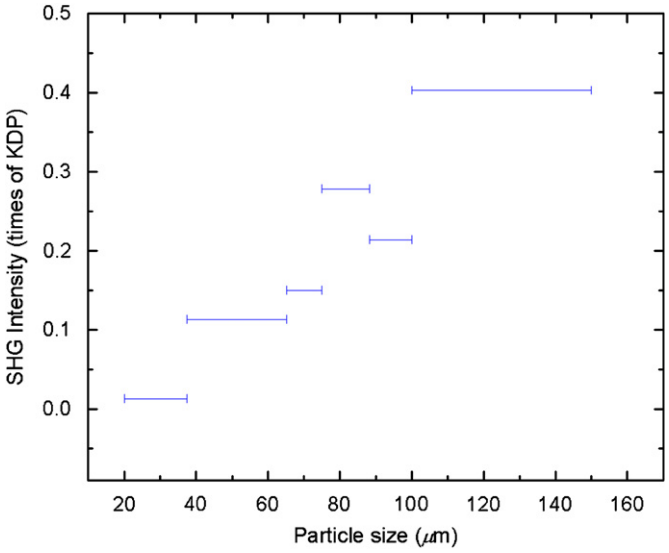

Fig. 3. SHG intensity versus particle size for crushed $K_2Fe_2B_2O_7$ crystal.

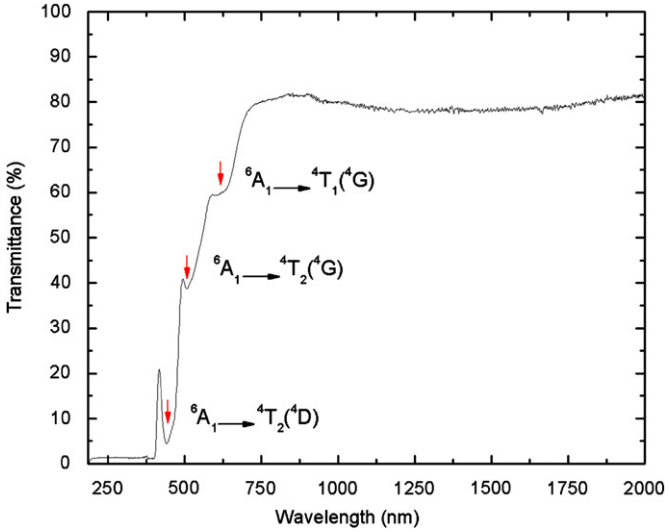

Fig. 4. Optical transmittance spectrum collected from $K_2Fe_2B_2O_7$ crystal. Three absorption bands are ascribed to *d–d* transitions of tetrahedrally coordinated Fe^{3+} ions: 442 nm ($^6A_1 \rightarrow {}^4T_2$ (^4D)), 520 nm ($^6A_1 \rightarrow {}^4T_2$ (^4G)) and 630 nm ($^6A_1 \rightarrow {}^4T_1$ (^4G)), respectively.

transparent in the 500–2000 nm region with three optical absorption bands attributed to *d–d* transitions of tetrahedrally coordinated Fe^{3+} ions. Both the powder SHG test and the calculation show that its SHG efficiency is about 0.4 times that of KDP. Spin-glass behavior is observed below 20 K which is attributed to geometrically magnetic frustration among Fe-ions in the triangular net.

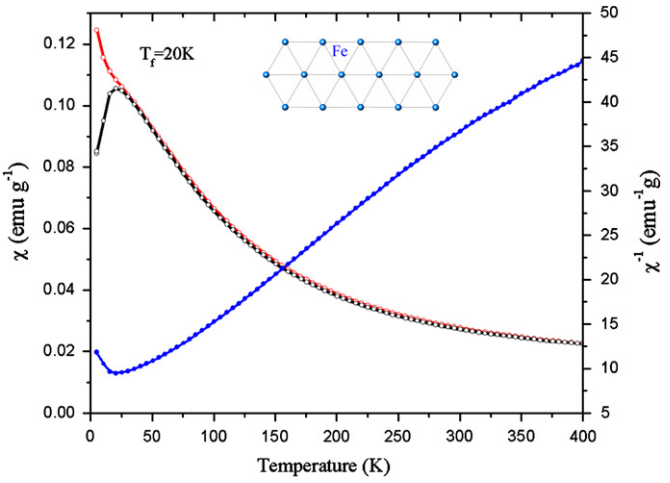

Fig. 5. Temperature dependence of the magnetic susceptibilities (FC and ZFC) in the temperature range 5–400 K of $K_2Fe_2B_2O_7$ under applied field of 1000 G, and their reciprocals (blue line) as a function of temperature (the inset shows the triangular Fe lattice in the *ab* plane). For interpretation of the references to colour in this figure legend, the reader is referred to the web version of this article.

Acknowledgment

This work is supported by the National Natural Science Foundation of China (Grant no. 90922036).

Appendix A. Supplementary material

Supplementary data associated with this article can be found in the online version at doi:10.1016/j.jssc.2010.03.037.

References

[1] G. Heller, A Survey of Structural Types of Borates and Polyborates, Topics in Current Chemistry, Springer, Berlin, 1986.
[2] P.H. Kemp, The Chemistry of Borates, Borax, London, 1956.
[3] P. Becker, Adv. Mater. 10 (1998) 979.
[4] C.T. Chen, B. Wu, A. Jiang, G. You, Sci. Sin. B 28 (1985) 235.
[5] C.T. Chen, Y.C. Wu, A. Jiang, B. Wu, G. You, R.K. Li, S. Lin, J. Opt. Soc. Am. B 6 (1989) 616.

[6] N.I. Leonyuk, L.I. Leonyuk, Prog. Cryst. Growth Charact. 31 (1995) 179.
[7] A.D. Mills, Inorg. Chem. 1 (1962) 960.
[8] D.A. Keszler, Curr. Opin. Solid State Mater. Sci. 1 (1996) 204.
[9] K.N. Boldyrev, E.P. Chukalina, N.I. Leonyuk, Phys. Solid State 50 (2008) 1681.
[10] E.A. Popova, N.I. Leonyuk, Phys. Rev. B 76 (2007) 054446.
[11] L.M. Dorozhkin, I.I. Kuratev, N.I. Leonyuk, T.I. Timchenko, A.V. shestakov, Pis'ma Zh. Tekh. Fiz. 7 (1981) 1297.
[12] D. Jaque, J. Alloys Compd. 204 (2001) 323.
[13] M. Huang, Y. Chen, X. Chen, Y. Huang, Z. Luo, Opt. Commun. 163 (2002) 208.
[14] Xueyuan Chen, Zundu Luo, D. Jaque, J.J. Romero, J. Garcia Sole, Yidong Huang, Aidong Jiang, Chaoyang Tu, J. Phys.: Condens. Matter 13 (2001) 1171.
[15] A.K. Zvezdin, S.S. Krotov, A.M. Kadomtseva, G.P. Vorob'ev, Yu.F. Popov, A.P. Pyatakov, L.N. Bezmaternykh, E.A. Popova, JETP Lett. 81 (2005) 272.
[16] A.N. Vasiliev, E.A. Popova, Low Temp. Phys. 32 (2006) 735.
[17] M.N. Popova, T.N. Stanislavchuk, B.Z. Malkin, L.N. Bezmaternykh, Phys. Rev. Lett. 102 (2009) 187403.
[18] (a) R. Wolfe, A.J. Kurtzig, R.C. LeCraw, J. Appl. Phys. 41 (1970) 1218;
(b) R. Diehl, Solid State Commun. 17 (1975) 743;
(c) P.A. Markovin, A.M. Kalashnikova, R.V. Pisarev, Th. Rasing, JETP Lett. 86 (2007) 712;
(d) B. Andlauer, J. Schneider, W. Wettling, Appl. Phys. 10 (1976) 189;
(e) Landolt-Börnstein, Numerical data and functional relationships in science and technology, In: H.P.J. Wijn (Ed.), Group III, vol. 27h, Springer, Berlin, 1993.
[19] R. Diehl, G. Brandt, Acta Crystallogr. B 31 (1975) 1662.
[20] (a) A.A. Demidov, N.P. Kolmakova, L.V. Takunov, D.V. Volkov, Physica B 398 (2007) 78;
(b) C. Ritter, A. Vorotynov, A. Pankrats, G. Petrakovskii, V. Temerov, I. Gudim, R. Szymczak, J. Phys.: Condens. Matter 20 (2008) 365209;
(c) J.A. Campa, C. Cascales, E. Gutierres-Puebla, M.A. Monge, I. Rasines, C. Ruz-Valero, Chem. Mater. 9 (1997) 237.
[21] (a) J.C. Fernandes, R.B. Guimaräes, M.A. Continentino, Phys. Rev. B 58 (1998) 287;
(b) M.A. Continentino, J.C. Fernandes, R.B. Guimaräes, Phys. Rev. B 9 (1999) 613;
(c) D.C. Freitas, M.A. Continentino, R.B. Guimaräes, J.C. Fernandes, Phys. Rev. B 79 (2009) 134437.
[22] *d–d* transitions of Fe^{3+} ions in Fe-doped $K_2Al_2B_2O_7$ crystal, in: Proceedings of the Fifth International Symposium on Laser, Scintillator and Non Linear Optical Materials (ISLNOM-5), Pisa, Italy, submitted to Optical Materials for publication.
[23] G.M. Sheldrick, Acta Crystallogr. A 64 (2008) 112.
[24] S.K. Kurtz, T.T. Perry, J. Appl. Phys. 39 (1968) 3798.
[25] (a) N. Ye, W. Zeng, B. Wu, C.T. Chen, Proc. SPIE 3556 (1998) 21;
(b) Z.G. Hu, Y. Mori, T. Higashiyama, M. Yoshimura, Y.K. Yap, Y. Kagebayashi, T. Sasaki, Proc. SPIE 3556 (1998) 156;
(c) Z.G. Hu, T. Higashiyama, M. Yoshimura, Y.K. Yap, Y. Mori, T. Sasaki, Jpn. J. Appl. Phys. 37 (1998) 1093.
[26] S.K. Filatov, R.S. Bubnova, Phys. Chem. Glasses 41 (2000) 216.
[27] (a) C.T. Chen, Y.C. Wu, R.K. Li, Int. Rev. Phys. Chem. 8 (1989) 65;
(b) C.T. Chen, Y.C. Wu, R.K. Li, J. Cryst. Growth 99 (1990) 790.
[28] D.N. Nikogosyan, Nonlinear Optical Crystals: A Complete Survey, Springer, New York, 2005, pp. 220.
[29] N. Umemura, M. Ando, K. Suzuki, E. Takaoka, K. Kato, Z.G. Hu, M. Yoshimura, Y. Mori, T. Sasaki, Appl. Opt. 42 (2003) 2716.
[30] D. Phanon, A. Mosset, I. Gautier-Luneau, J. Mater. Chem. 17 (2007) 1123–1130.
[31] A.P. Ramirez, Annu. Rev. Mater. Sci. 24 (1994) 453.
[32] A.P. Ramirez, Czech. J. Phys. 46 (1996) 3247.
[33] John E. Greedan, J. Mater. Chem. 11 (2001) 37.
[34] R.K. Li, C.T. Chen, C. Greaves, Phys. Rev. B 66 (2002) 052405.
[35] R.K. Li, C. Greaves, Phys. Rev. B 68 (2003) 172403.
[36] R.K. Li, C. Greaves, Phys. Rev. B 70 (2004) 132411.